Bainite transformation kinetics
Part 1 Modified model

G. I. Rees and H. K. D. H. Bhadeshia

An earlier model for the overall transformation kinetics of bainite has been corrected and modified to be consistent with known details of the mechanisms of bainitic nucleation and growth. A comparison with published experimental data shows that the model is capable of accurately representing the development of transformation as a function of alloy chemistry and temperature.

MST/1627

Manuscript received 3 February 1992. *The authors are in the Department of Materials Science and Metallurgy, University of Cambridge/JRDC, Cambridge.*

Introduction

A large increase is currently apparent in the demand for bainitic steels, cast irons, and weld deposits for a wide variety of applications ranging from rail steels to accelerated cooled low carbon steels for structural engineering.[1,2] The research effort backing these developments could benefit greatly from kinetic theory capable of predicting the bainitic microstructures as a function of alloy chemistry and thermomechanical treatment.

The problem is complicated by the fact that there are several microstructural scales to consider (Fig. 1). The transformation usually begins at the austenite grain surfaces with the nucleation and growth of individual platelets of ferrite. The displacements that occur during growth represent a shape change which is an invariant plane strain (IPS) with a large shear component.[3] The growth of the platelet is stifled by the dislocation debris created as the IPS shape change is plastically accommodated.[4,5] The platelets thus grow to a limited size, which is usually smaller than the austenite grain size. Further transformation occurs by the formation of new, parallel platelets in clusters known as sheaves; the platelets are therefore called the 'subunits' of the sheaf.[6]

It is thought that the subunits grow without diffusion, but that any excess carbon in the ferrite is soon afterwards partitioned into the residual austenite.[7,8] The indications are that the time required to grow a subunit is small relative to that needed to nucleate successive subunits.[9,10] The growth rate of individual subunits[9] is known to be much faster than the lengthening rate for sheaves.[8,10–13]

The overall transformation kinetics include the simultaneous growth and impingement of many different sheaves. A further complication is that carbide precipitation may eventually occur from the carbon enriched residual austenite, or, in the case of lower bainite, from the supersaturated ferrite. Carbide precipitation is not addressed in this study, which is confined to situations where the use of alloying additions such as silicon prevents it. Fortunately, it transpires that the vast majority of bainitic steels under active consideration for major applications do not involve carbide precipitation.

The purpose of the work presented here was to develop a model for the overall transformation kinetics, based on the mechanism of the bainite transformation. Such a model was last attempted in 1982.[14] As seen below, it contains a number of important discrepancies.[14]

Problems with earlier theory

In steels containing a relatively large concentration of silicon (>1·5 wt-%), the precipitation of carbides can be suppressed, especially when the transformation temperature is in the upper bainite range. We have noted that bainitic ferrite subunits grow without diffusion, but that any excess carbon is soon afterwards partitioned into the residual austenite. This makes it more difficult for subsequent subunits to grow, as the austenite becomes stabilised by its increased carbon concentration. The maximum extent to which the bainite reaction can proceed is therefore determined by the composition of the residual austenite. Bainite growth must cease when the free energies of austenite and ferrite of identical composition become equal. The locus of all points on a temperature–carbon concentration plot, where austenite and ferrite of identical chemistry have equal free energies, is called the T_0 curve; when this is modified to allow for the stored energy of bainite (~400 J mol^{-1}),[5,8] the locus becomes the T_0' curve. Thus, the diffusionless growth of bainitic ferrite becomes impossible when the carbon concentration of the residual austenite reaches the T_0' concentration. This maximum volume fraction is termed θ. The normalised volume fraction ξ is then defined as

$$\xi = v/\theta \quad . \quad . \quad . \quad . \quad . \quad . \quad . \quad . \quad . \quad . \quad . \quad . \quad . \quad . \quad . \quad (1)$$

where v is the actual volume fraction of bainitic ferrite.

The activation energy for the nucleation of bainite is known to be directly proportional to the driving force for transformation.[15] This is consistent with the theory for martensite nucleation,[16,17] although it is required that carbon should partition into the austenite during bainite nucleation.[15] The nucleation mechanisms of Widmanstätten ferrite and bainite are considered to be identical; a potential nucleus can develop into either phase depending on whether or not an adequate driving force is available for the growth of bainite at the transformation temperature concerned. On this basis, it is possible to define a universal nucleation function of temperature G_N which is applicable to all steels. In a given steel, nucleation first becomes possible at a detectable rate below a temperature W_S (the Widmanstätten ferrite start temperature), at which the magnitude of the maximum nucleation free energy change ΔG_m for the steel exceeds that given by G_N.[15,18,19]

According to the original overall transformation kinetics theory developed by Bhadeshia,[14] the nucleation rate of ferrite per unit volume I, at any temperature T, can be expressed as a multiple of the nucleation rate at the W_S temperature, I_{W_S}

$$I = I_{W_S} \exp\left[-\frac{C_2 \Delta T}{RTW_S} - \frac{C_3}{R}\left(\frac{\Delta G_m}{T} - \frac{G_N}{W_S}\right)\right] \quad . \quad . \quad . \quad (2)$$

where ΔG_m represents the maximum possible free energy change on nucleation, and G_N is the value of the universal curve representing the minimum necessary free energy change for displacive nucleation of ferrite at the W_S temperature. C_2 and C_3 are empirical constants. ΔG_m is a function of the volume fraction of ferrite, since carbon

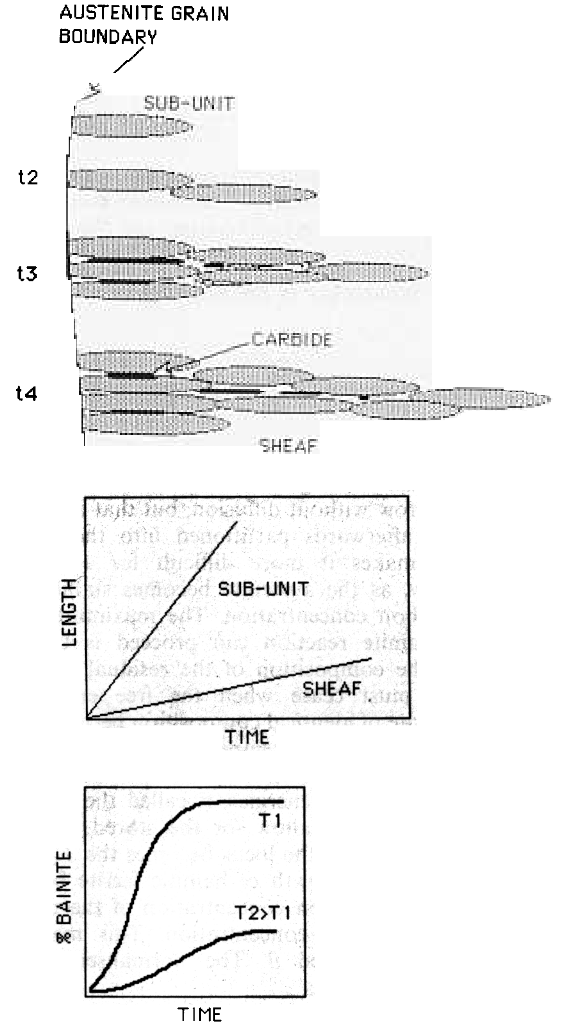

1 **Schematic of variety of stages of development of bainitic microstructure**

enrichment of the untransformed austenite will lower the magnitude of the free energy change as the volume fraction of ferrite increases. This effect is modelled as

$$\Delta G_m = \Delta G_m^0[1 - (C_4\theta\xi/C_3)] \quad \ldots\ldots (3)$$

where ΔG_m^0 is the initial value of ΔG_m, and C_4 is an empirical constant.

The effect of autocatalysis, i.e. the increase in number density of nucleation sites as the volume fraction of ferrite increases, is modelled as

$$I_{W_S} = I_0(1 + \beta\theta\xi) \quad \ldots\ldots (4)$$

where β is the empirical autocatalysis constant. At the onset of transformation, the increment dv of volume fraction of ferrite that forms between times t and $t + dt$ is given by

$$dv = \theta d\xi = Iu\, dt \quad \ldots\ldots (5)$$

where u is the volume of a bainitic subunit and I is the nucleation rate per unit volume.

At later stages in the transformation, as the volume of austenite available for transformation has decreased, it is necessary to consider the increment in the 'extended volume' dv_e,[20] which accounts for the formation of 'phantom' nuclei within regions of ferrite already transformed. This enables the use of the nucleation rate of bainite per unit volume of austenite, despite the fact that the volume of austenite is changing, provided that the extended volume increment is related to the real volume increment. This is done as follows

$$dv = (1 - \xi)\, dv_e \quad \ldots\ldots (6)$$

where

$$dv_e = Iu\, dt \quad \ldots\ldots (7)$$

which gives

$$\theta d\xi = (1 - \xi)Iu\, dt \quad \ldots\ldots (8)$$

Substituting the expressions for the nucleation rate of bainite gives

$$\theta\frac{d\xi}{dt} = uI_0(1 - \xi)(1 + \beta\theta\xi)\exp(\Gamma\xi) \times \exp\left[-\frac{C_2\Delta T}{RTW_S} - \frac{C_3}{R}\left(\frac{\Delta G_m^0}{T} - \frac{G_N}{W_S}\right)\right] \quad \ldots (9)$$

where u is the average volume of a single subunit and

$$\Gamma = \frac{C_4\Delta G_m^0}{RT} \quad \ldots\ldots (10)$$

The equation can be integrated by separating the variables

$$\int_0^\xi \frac{A d\xi}{1 - \xi} + \int_0^\xi \frac{B d\xi}{1 + \beta\theta\xi} + C\int_0^\xi \exp(-\Gamma\xi)\, d\xi = \frac{I_0}{\theta}\exp\left[-\frac{C_2\Delta T}{RTW_S} - \frac{C_3}{R}\left(\frac{\Delta G_m^0}{T} - \frac{G_N}{W_S}\right)\right]\int_0^t dt \quad \ldots\ldots (11)$$

where A, B, and C are constants arising from the separation of the differential equation into partial fractions. ΔT is defined as $T - W_S$.

An analytical solution is obtained which gives the time t taken to form a normalised volume fraction ξ at the reaction temperature T

$$t = \frac{\theta[-A\ln(1 - \xi) + (B/\beta\theta)\ln(1 + \beta\theta\xi) + (C/\Gamma)(1 - e^{-\Gamma\xi})]}{uI_0\exp\left[-\frac{C_2\Delta T}{RTW_S} - \frac{C_3}{R}\left(\frac{\Delta G_m^0}{T} - \frac{G_N}{W_S}\right)\right]} \quad \ldots\ldots (12)$$

After optimisation of the model, the best fit values of the empirical constants were found to be[14]

$uI_0 = 1{\cdot}234 \times 10^{-4}\ s^{-1}$
$C_2 = 27\,910\ J\ mol^{-1}$
$C_3 = 3{\cdot}679$
$C_4 = 11$
$\beta = 200$

The present study began with the use of this model as a means to the prediction of weld metal microstructures, but it was soon realised that there are certain important errors.

PREDICTION ERRORS

A thorough assessment of the model was made, using thermodynamic parameters and theory (necessary to calculate ΔG_m, for example) outlined when it was first proposed.[14] As is shown in Fig. 2, the original model incorrectly predicts that, at the same transformation temperature, a steel with a high manganese content will transform at a faster rate than a more lightly alloyed steel. This prediction is contrary to experience. Table 1 gives the compositions of the steels used for the comparison calculation, which was performed for a reaction temperature of 470°C. This temperature was calculated to lie between the bainite start and martensite start temperatures for both alloys. The compositions were chosen to be consistent with the welding alloys that are currently under investigation. The values of ΔG_m^0, G_N, and W_S, together with the predicted B_S and M_S, were calculated using theory outlined in Ref. 15.

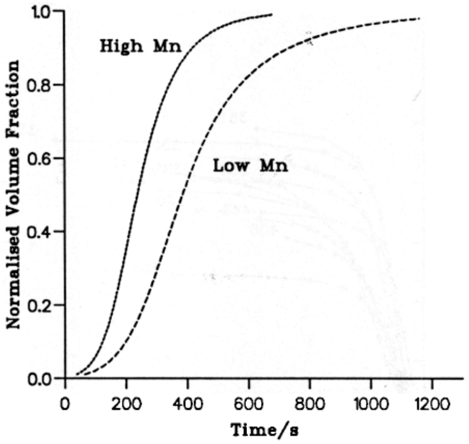

2 Relative reaction rates of high manganese and low manganese steel, as predicted by original bainite transformation kinetics model;[14] steel compositions are given in Table 1

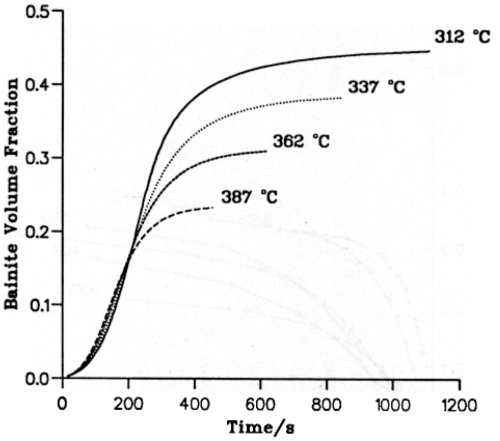

3 Predicted isothermal transformation curves for 300 M steel (Table 2) calculated using original bainite transformation kinetics model:[14] curves show that initial reaction rate is predicted to decrease with decreasing temperature

The model also predicted, for all steels, a deceleration in transformation rate as the undercooling below W_S increased. An example is presented in Fig. 3, which shows the calculated transformation curves for the isothermal formation of bainite in 300 M steel (Table 2) at various temperatures within the bainite transformation range. The initial reaction rate is predicted to decrease as the isothermal transformation temperature decreases, despite the fact that driving force increases as temperature decreases. The calculations also contradict experimental data for 300 M, discussed below, which show the opposite trend.

THEORETICAL PROBLEMS

A key assumption used in the derivation of the universal nucleation function G_N was that at the highest temperature at which ferrite can nucleate by a displacive mechanism (i.e. W_S), all steels should have an identical nucleation rate.[15] The original bainite kinetics model[14] is not, in general, consistent with this assumption. This can be shown by comparing the nucleation rates of two steels, A and B, at their W_S temperatures, W_{SA} and W_{SB} respectively. The G_N function represents the minimum driving force necessary to initiate nucleation of ferrite by a displacive mechanism. It is found to be a linear function of temperature.[15] At the W_S temperature, ΔG_N is given by

$$G_N = pW_S - r \qquad (13)$$

where p and r are positive constants. If G_{NA} and G_{NB} represent the values of G_N at W_{SA} and W_{SB} respectively

$$G_{NA} = pW_{SA} - r \qquad (14)$$

$$G_{NB} = pW_{SB} - r \qquad (15)$$

where[19]

$p = 3{\cdot}6375$
$r = 2540\ \mathrm{J\ mol^{-1}}$

It follows from equation (2) that the ratio of nucleation rates in the two steels at their respective W_S temperatures is given by

$$\frac{I_A}{I_B} = \exp\left[-\frac{(C_2 - C_3 r)(W_{SB} - W_{SA})}{R W_{SA} W_{SB}}\right] \qquad (16)$$

From equation (16) it can be seen that unless

$$C_2 = C_3 r \qquad (17)$$

different steels will not have the same nucleation rate at their W_S temperature. The values of the terms derived for the original theory[14] are

$C_2 = 27\,910\ \mathrm{J\ mol^{-1}}$
$C_3 = 3{\cdot}679$
$r = 2540\ \mathrm{J\ mol^{-1}}$.

which clearly do not satisfy this condition.

A further difficulty was identified in the modelling of the effect of carbon enrichment of untransformed austenite on the $\gamma \rightarrow \alpha$ free energy change

$$\Delta G_m = \Delta G_m^0 (1 - C_4 \theta \xi / C_3) \qquad (18)$$

with the value of C_4/C_3 equal to 2·98. This equation predicts that the value of ΔG_m will be positive after a volume fraction of bainite of 0·34 has formed, regardless of temperature or alloy chemistry.

Bainite is observed to grow until the carbon content of the untransformed austenite reaches the value given by T_0' for the steel. The limiting volume fraction of bainite is thus a function of temperature and alloy chemistry. It is not reasonable, therefore, for transformation to cease when a volume fraction of 0·34 is achieved. Indeed, the isothermal transformation data used for the investigation of the

Table 1 Steel compositions (wt-%) and calculated M_S and B_S temperatures (°C) used for comparison of predicted reaction rates

Steel	C	Si	Mn	Ni	Mo	Cr	B_S	M_S
1 (high Mn)	0·06	0·5	2·0	2·0	0·4	0·6	478	406
2 (low Mn)	0·06	0·5	1·0	2·0	0·4	0·6	565	455

Table 2 Composition (wt-%) of steels used for determination of reaction kinetics of bainite

Steel	C	Si	Mn	Ni	Mo	Cr	V
Fe Mn Si C	0·22	2·03	3·00	0·00	0·00	0·00	0·00
Fe Ni Si C	0·39	2·05	0·00	4·08	0·00	0·00	0·00
300 M	0·44	1·74	0·67	1·85	0·83	0·39	0·09

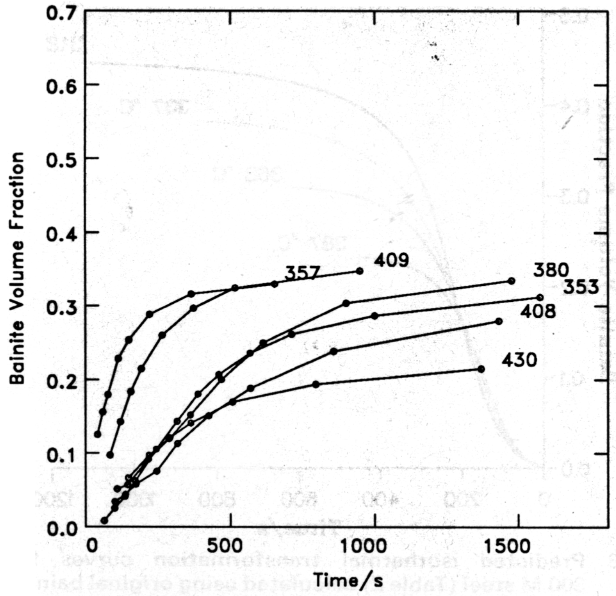

Plot of isothermal transformation kinetics data obtained for Fe–Mn–Si–C steel, as used for optimisation of original kinetics model[14]

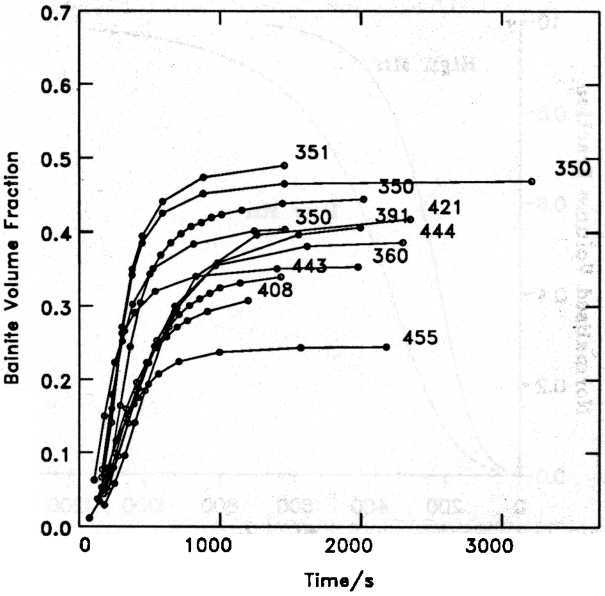

5 Plot of isothermal transformation kinetics data obtained for Fe–Ni–Si–C steel, as used for optimisation of original kinetics model[14]

original model show many cases where the volume fractions are much higher than 0·34. This can be seen in Figs. 4–6, which show the data for the steels Fe–Mn–Si–C, Fe–Ni–Si–C, and 300 M.[14]

Development of new model

NUCLEATION RATE AT W_S

To ensure that the activation energy for nucleation remains directly proportional to ΔG_m,[14] and imposing the condition that the nucleation rate at W_S is constant for all steels, the expression for the nucleation rate of bainite is modified to

$$I = K_1 \exp\left(-\frac{K_2}{RT} - \frac{K_2 \Delta G_m}{rRT}\right) \qquad (19)$$

where K_1 and K_2 are constants, denoted as such in order to avoid confusion with the constants of the original theory. K_1 represents the number density of potential sites for nucleation. At W_S, equation (19) becomes

$$I = K_1 \quad . \; . \; . \; . \; . \; . \; . \; . \; . \; . \; . \; . \; . \; . \; . \; . \quad (20)$$

regardless of the alloy composition.

EFFECT OF CARBON PARTITIONING ON FREE ENERGY CHANGE

As transformation proceeds, it becomes necessary to account for the decrease in driving force due to the carbon enrichment of untransformed austenite. The effect of autocatalysis also becomes important.

As mentioned above, the formation of bainite can occur only when the thermodynamic criteria for both nucleation and growth are satisfied. At the onset of transformation the criterion for nucleation is

$$\Delta G_m < G_N \quad . \; . \; . \; . \; . \; . \; . \; . \; . \; . \; . \; . \; . \; . \quad (21)$$

and the growth criterion is that the driving force for transformation without a composition change exceeds the stored energy of bainite

$$\Delta G^{\gamma \rightarrow \alpha} < -400 \text{ J mol}^{-1} \quad . \; . \; . \; . \; . \; . \; . \; . \; . \quad (22)$$

Equation (22) defines the T_0' curve, but both the nucleation and growth criteria must be satisfied during transformation. As the austenite carbon concentration increases during transformation, the magnitude of both ΔG_m and $\Delta G^{\gamma \rightarrow \alpha}$ will decrease. Eventually the reaction will cease when one criterion is not satisfied. The value of θ, the maximum allowable volume fraction at the reaction temperature, is taken as the ferrite volume fraction when reaction ceases, regardless of whether termination is by a failure of the nucleation or the growth criterion.

Let x_{N_0} and $x_{T_0'}$ represent the austenite carbon concentration when the nucleation and growth criteria respectively fail. If the driving force is assumed to vary linearly with the extent of reaction, between its initial value ΔG_m^0 and its final value when the reaction terminates, then

$$\Delta G_m = \Delta G_m^0 - \xi(\Delta G_m^0 - G_N) \quad . \; . \; . \; . \; . \; . \; . \; . \quad (23)$$

This equation is inaccurate when $x_{N_0} > x_{T_0'}$, but this is not a significant problem, as the model also includes a growth criterion in which reaction ceases when the fraction θ is achieved. The form of the equation has an additional advantage in that the linear function of ξ preserves the ability to integrate the final differential equation representing the overall transformation kinetics analytically. A comparison of the x_{N_0} and $x_{T_0'}$ curves for the steel 300 M is shown in Fig. 7, demonstrating that they are in fact quite close and that both lie well below the Ae_3' curve, which is the $(\alpha + \gamma)/\gamma$ paraequilibrium phase boundary.

AUTOCATALYSIS

Steels with a high carbon concentration eject more carbon from the newly transformed ferrite than lower carbon steels. The buildup of carbon at the ferrite/austenite interfaces causes a temporary local decrease in the driving force for diffusionless transformation. The process of further nucleation on the previously formed plates (i.e. autocatalysis) is inhibited by this carbon buildup, suggesting that the autocatalysis factor used in the kinetics model should in some way be dependent on the overall carbon concentration of the alloy. For simplicity, it is assumed that

$$\beta = \lambda_1(1 - \lambda_2 \bar{x}) \quad . \; . \; . \; . \; . \; . \; . \; . \; . \; . \; . \quad (24)$$

where $\bar{x}$ represents the mean carbon concentration of the alloy, and β is the autocatalysis factor (equation (4)). λ_1 and λ_2 are empirical constants. In this way, the effect of

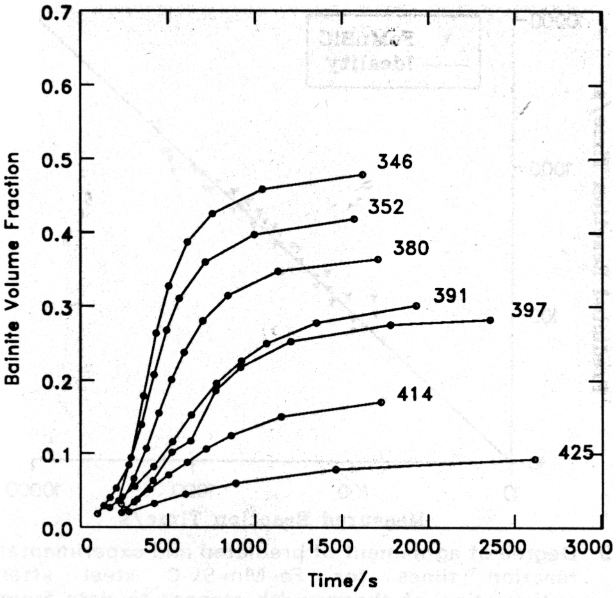

6 Plot of isothermal transformation kinetics data obtained for 300 M steel, as used for optimisation of original kinetics model[14]

autocatalysis is less for high carbon steels than for those with lower carbon content. The additional nucleation sites introduced as transformation proceeds are then specified by equation (4).

EFFECT OF AUSTENITE GRAIN SIZE

The original model did not include a specific austenite grain size effect. The nucleation rate of a grain boundary nucleated transformation can be assumed to be proportional to the surface area of austenite grain boundaries per unit volume S_V. This is because the number of suitable sites for nucleation is expected to be directly proportional to the surface area of γ/γ grain boundaries within the sample.

Stereological theory relates S_V to the mean linear intercept $\bar{L}$ of a series of random lines with the austenite grain boundaries,[21] by

$$S_V = 2/\bar{L} \qquad (25)$$

In the new expression for the nucleation rate of bainite, the term K_1 will be a function of the austenite grain size, as expressed by the mean linear intercept

$$K_1 = (\bar{L}K'_1)^{-1} \qquad (26)$$

where K'_1 is an empirical constant.

FINAL EXPRESSION

The modifications discussed above can be incorporated into a new model as follows. The volume fraction increment between times t and $t + \mathrm{d}t$ is

$$\theta \mathrm{d}\xi = (1 - \xi)uI\,\mathrm{d}t \qquad (27)$$

where u is the subunit volume and I is the nucleation rate of bainite per unit volume. The expression for the nucleation rate of bainite can be substituted into this equation, giving a differential equation for the overall transformation rate of bainite

$$\frac{\mathrm{d}\xi}{\mathrm{d}t} = \frac{uK_1}{\theta}(1 - \xi)(1 + \beta\theta\xi) \times \exp\left[-\frac{K_2}{RT}\left(\quad + \frac{\Delta G^0_{\mathrm{m}}}{r} \right) + \Gamma_2\xi \right] \qquad (28)$$

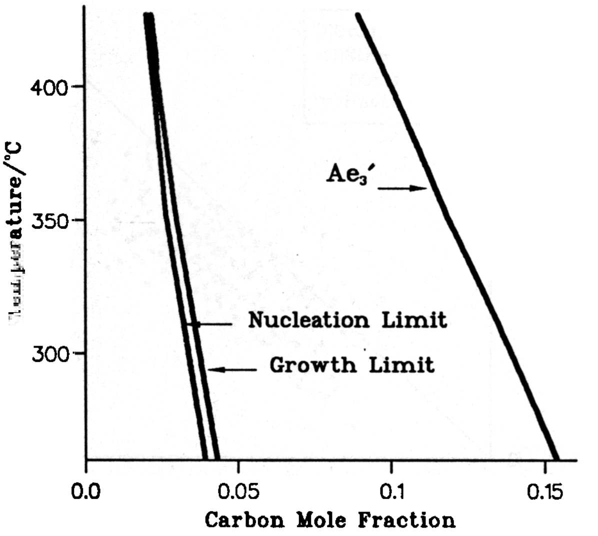

7 Comparison of x_{N_0} and $x_{T'_0}$ curves for 300 M steel: Ae_3' curve represents paraequilibrium $(\alpha + \gamma)/\gamma$ phase boundary

where Γ_2 is given by

$$\Gamma_2 = \frac{K_2(\Delta G^0_{\mathrm{m}} - G_{\mathrm{N}})}{rRT} \qquad (29)$$

The solution of equation (29) has the same form as in the previous theory, i.e.

$$t = \frac{\theta[-A\ln(1 - \xi) + (B/\beta\theta)\ln(1 + \beta\theta\xi) + (C/\Gamma_2)(1 - \mathrm{e}^{-\Gamma_2\xi})]}{uK_1\exp\left(-\frac{K_2}{RT} - \frac{K_2\Delta G^0_{\mathrm{m}}}{rRT} \right)} \qquad (30)$$

The constants were determined by optimising the theory using the same data as used by Bhadeshia.[14] In this way the two theories can be directly compared.

INTERPRETATION OF EXPERIMENTAL DATA

The compositions of the steels used for the original analysis are given in Table 2. The experimental data were obtained by dilatometry over various temperatures within the bainitic transformation range. These length change data were analysed using the procedure outlined in Ref. 14. For each individual reaction the data were then normalised with respect to the maximum extent of reaction, to produce datasets of normalised volume fraction ξ versus time t, for the purpose of evaluating the unknown constants.

Figures 4–6 show plots of the experimental isothermal transformation kinetics data obtained by Bhadeshia for the Fe–Mn–Si–C, Fe–Ni–Si–C, and 300 M steels.[14] Of the three steels, 300 M shows the most consistent behaviour; the other two occasionally show odd results for transformation under similar conditions. A mathematical model obviously cannot reproduce results that are intrinsically inconsistent in this way.

In the case of the Fe–Mn–Si–C steel, two transformation runs, at 409 and 357°C, gave particularly dubious results. The optimisation of the model was carried out after discarding those points, though the calculations were also carried out incorporating the rogue points in order to determine their effect on the overall agreement.

GRAIN SIZE MEASUREMENT

The original model gives no account of the effect of the austenite grain size on transformation kinetics. To incorporate this effect, the austenite grain sizes produced in the three steels after austenitisation for 5 min at 1000°C were

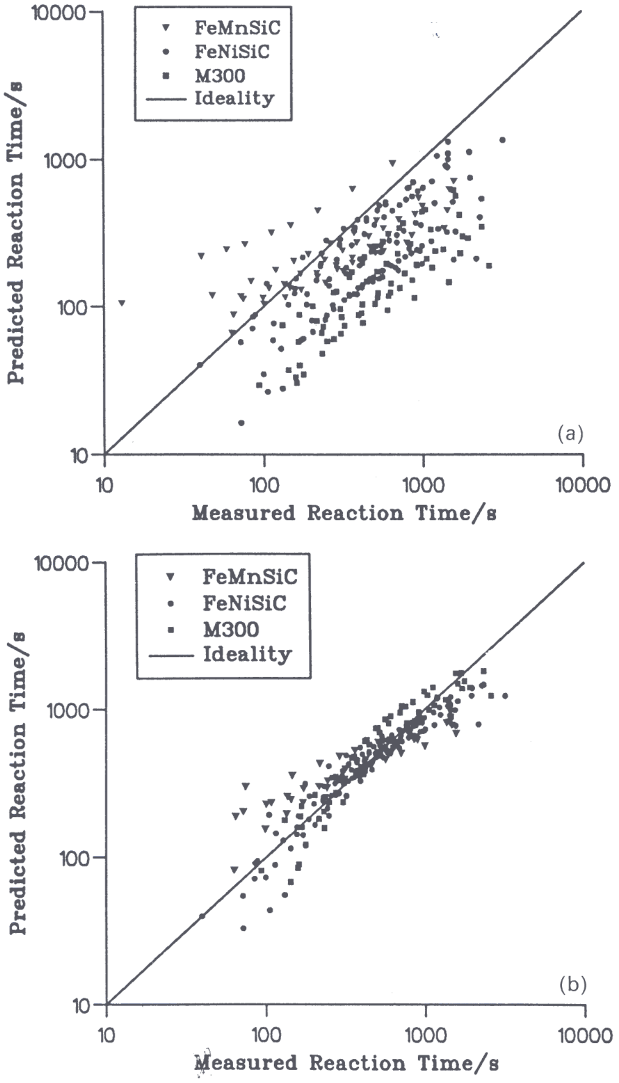

a original theory; *b* new theory

8 Comparison of predicted and experimentally determined reaction times for bainite reaction in high silicon steels

measured. The samples were quenched after austenitisation and then tempered for 1 h at 600°C, in order to enhance the delineation of the original austenite grains. The specimens were mounted, ground, polished, and etched in 2% nital for optical metallography. Grain size was represented by the mean linear intercept of a series of random lines with the grain boundaries, on scanning electron micrographs of the microstructure. Table 3 gives the results of the mean linear intercept measurements. The number of measurements was in each case 100, giving a statistical error of about ±10%.

NUMERICAL ANALYSIS

To utilise the new model, it is necessary to determine four constants: K'_1/u, K_2, λ_1, and λ_2. This is one fewer than in the original model, because of the new condition which ensures that the nucleation rate is constant at W_S. Values of the constants were adjusted to give the best agreement between the theory and the experimental data, subject to the condition that the expression

$$\sum [\ln(t_p) - \ln(t_m)] \quad \quad (31)$$

is minimised, where t_p denotes the predicted reaction time and t_m denotes the experimental reaction time. The logarithms of these terms are taken because otherwise the error at larger time dominates the sum. A computer algorithm was developed to search downhill for a minimum to the above expression. The program was terminated when no significant improvements could be achieved.

In order to investigate the origin of any scatter in the agreement between predicted and experimental reaction times, the model was optimised with respect to the data from each individual steel as well as the combined data from all the steels. In the case of the computer runs involving just one steel there is no variation in the carbon content; the constant λ_2 was therefore set to zero.

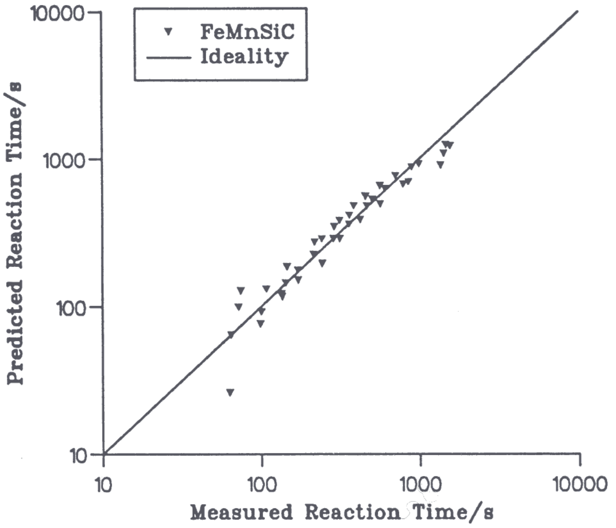

9 Degree of agreement of predicted and experimental reaction times for Fe–Mn–Si–C steel after optimisation of theory with respect to data from this steel alone

Results

Figure 8 shows plots of predicted versus experimental reaction times using the original and the new theory. The results for individual steels are shown in Figs. 9–11. These plots correspond to steels Fe–Mn–Si–C, Fe–Ni–Si–C, and 300 M. The calculations are summarised in Table 4.

The effect of including the rogue data from the Fe–Mn–Si–C steel is shown in Fig. 12*a*, which should be compared with Fig. 8*b*. There is a deterioration in the overall agreement. Figure 12*b* (to be compared with Fig. 9) shows how the rogue data reduce the agreement with theory, for

Table 3 Mean linear intercept values for austenite grain size of high silicon steels after austenitisation at 1000°C for 5 min

Steel	Mean linear intercept, μm
Fe–Mn–Si–C	47 ± 5
Fe–Ni–Si–C	52 ± 6
300 M	86 ± 9

Table 4 Best fit values of constants after optimisation of new theory using different datasets

Dataset	K'_1/u, m² s	K_2, J mol^{-1}	λ_1	λ_2
Combined data	$33{\cdot}90 \times 10^6$	$2{\cdot}065 \times 10^4$	139·00	25·46
Fe–Mn–Si–C	$38{\cdot}76 \times 10^6$	1·925	4·756	0·00
Fe–Ni–Si–C	$20{\cdot}28 \times 10^6$	$2{\cdot}907 \times 10^4$	90·822	0·00
300 M	$12{\cdot}308 \times 10^6$	$3{\cdot}767 \times 10^4$	141·66	0·00

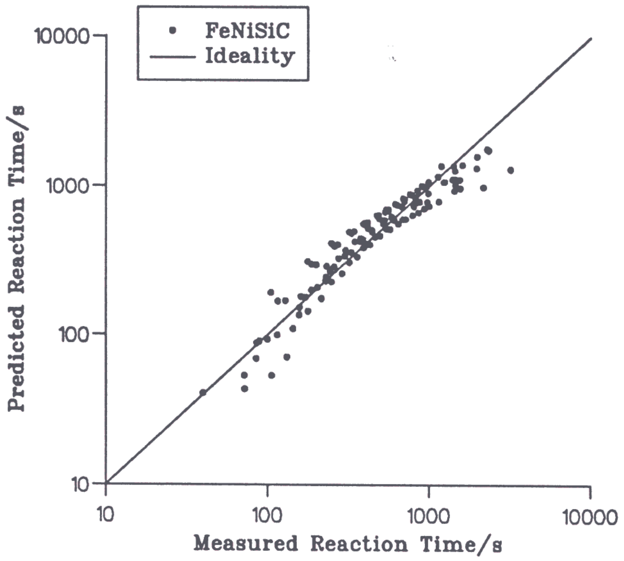

10 Degree of agreement of predicted and experimental reaction times for Fe–Ni–Si–C steel after optimisation of theory with respect to data from this steel alone

the Fe–Mn–Si–C on its own. Table 5 gives the best fit values for the constants when the rogue data are included in the numerical analysis.

APPLICATION OF NEW THEORY

The improvements due to the new analysis can be highlighted by comparison with the original model. Figure 13 shows the predicted transformation behaviour of steels 1 and 2 at 470°C. As can be seen, the high manganese steel is now predicted to transform more slowly than steel 2, which has a smaller manganese concentration. Trends due to alloying element concentrations are therefore correctly predicted, unlike the data shown in Fig. 2. Figure 14 shows the effect of temperature on the transformation behaviour of 300 M. The reaction kinetics are shown to increase with decreasing temperature, as was observed experimentally, again correcting the erroneous prediction by the original model. It can be seen by comparing the plots in Fig. 8 that the new theory gives a significantly better agreement between the measured and predicted reaction times. Data from each of the individual steels are also shown to be broadly consistent with the theory, though the constants derived by individual optimisation differ from those consistent with the best overall fit. The reasons for this effect are not clear; it is particularly worrying that the best fit constants for the Fe–Mn–Si–C steel are so different from those for the other alloys. Nevertheless, the form of the transformation curves is clearly well represented by the model.

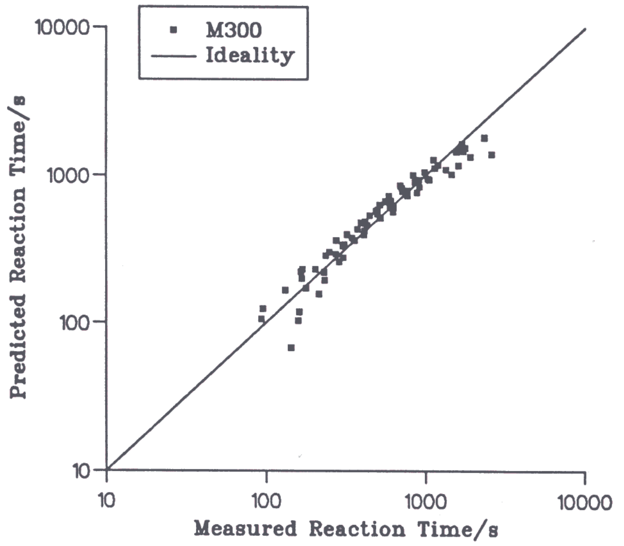

11 Degree of agreement of predicted and experimental reaction times for 300 M steel after optimisation of theory with respect to data from this steel alone

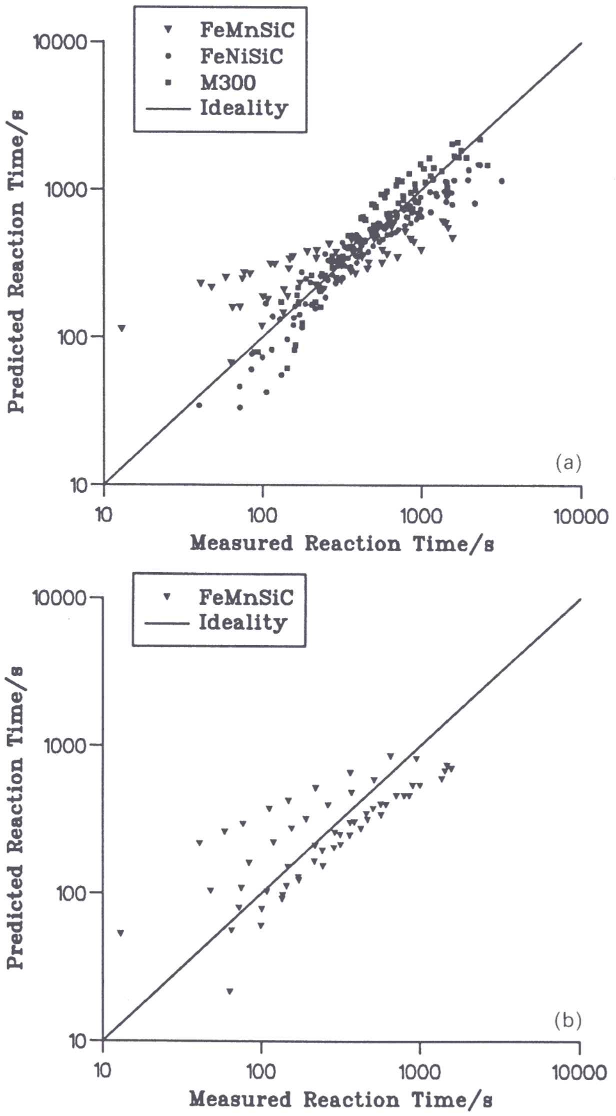

a deterioration in overall agreement; *b* best fit for Fe–Mn–Si–C steels considered alone

12 Effect on degree of agreement with new model of including rogue data from Fe–Mn–Si–C

The results can be summarised in a TTT diagram. Figure 15 shows the predicted TTT diagrams for steel 1 and steel 2, illustrating the fact that the manganese rich steel transforms more slowly and that the reaction kinetics increase with decreasing temperature. A notable feature is

Table 5 Best fit values of constants when numerical analysis includes rogue data in Fe–Mn–Si–C experiments

Dataset	K'_1/u, m^2 s	K_2, J mol^{-1}	λ_1	λ_2
Combined data	$19{\cdot}92 \times 10^6$	$2{\cdot}624 \times 10^4$	259·20	39·69
Fe–Mn–Si–C	$19{\cdot}18 \times 10^6$	$6{\cdot}395 \times 10^3$	9·696	0·00

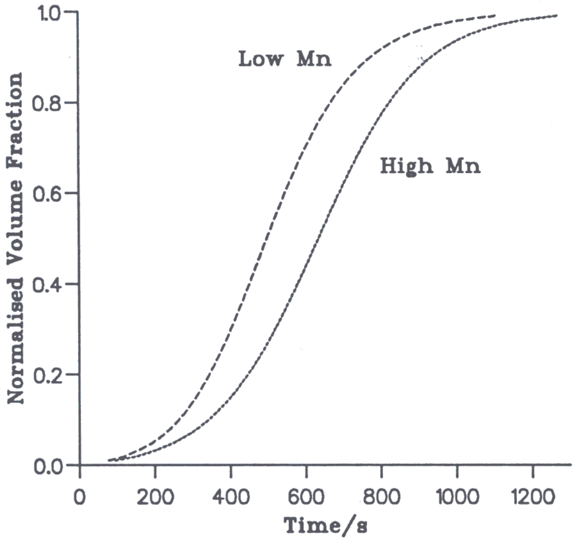

13 Comparison of predicted reaction rates of steels 1 and 2 (Table 1) at 470°C using new bainite kinetics model: higher manganese content of steel 2 results in slower transformation, as expected, correcting error in original model

that the predicted curves do not show the *C*-curve shape seen in some experimental diagrams. Published TTT curve atlases reveal that this is not unexpected in high hardenability alloys, although it is also worth noting that the present analysis takes no account of carbide precipitation, so that detailed comparisons are not in general possible. Most of the TTT curve data pertain to steels not used in the bainitic condition; modern bainitic steels are designed to avoid carbide precipitation.

The absence of a *C*-shape could be real (as indicated by the experimental data for 300 M steel) or due to other factors that have been neglected. It has been consistently reported that the apparent thickness of bainitic subunits varies as a function of the transformation temperature.[8,22,23] It is not possible, however, to model this size variation without relaxing the condition that the steels have the same nucleation rate at W_S, though we have verified that such size variation would indeed result in a *C*-shaped TTT curve.

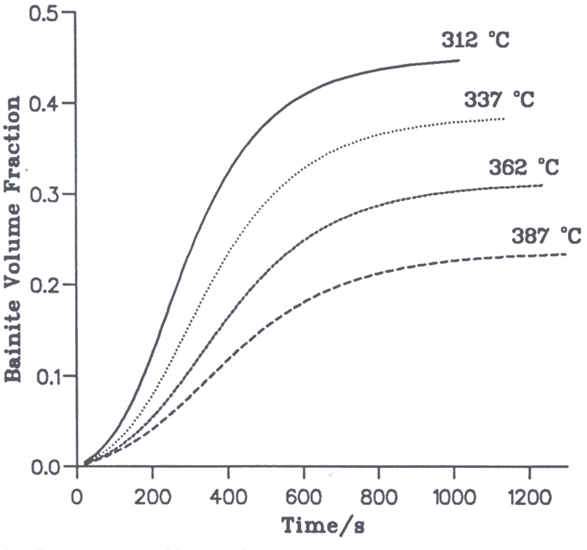

14 Predicted effect of temperature on transformation of 300 M steel: kinetics are predicted to increase with decreasing temperature, as observed experimentally, correcting error in original model

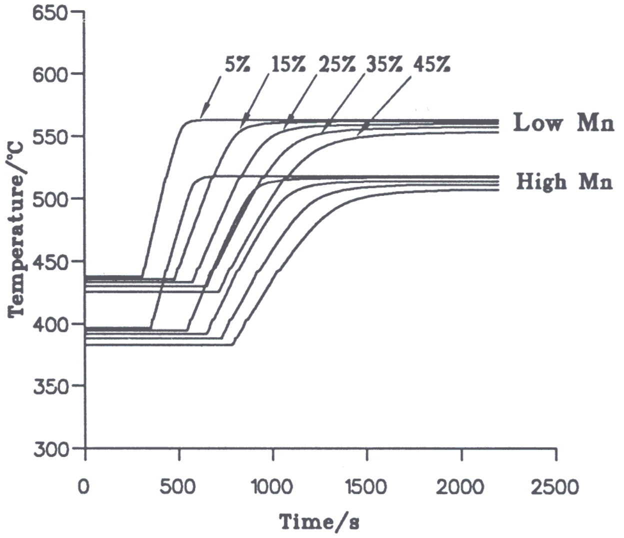

15 Comparison of predicted time–temperature–transformation (TTT) curves for steels 1 and 2 using new model: curves illustrate prediction that highly alloyed steels will react more slowly than lightly alloyed steels and that reaction rate increases with undercooling below B_S

Conclusions

An earlier model for the overall transformation kinetics of bainite in steels where carbide precipitation can be suppressed has been corrected and refined to be consistent with the known mechanisms of bainite nucleation and growth. The new model estimates the rate of reaction more precisely; it has a greater degree of internal consistency and one fewer disposable constant. Theory and experiment can be made to agree well by optimising the values of four parameters, of which two describe autocatalysis and two describe the nucleation phenomena. It is suggested that these parameters can be used for all steels (where carbide formation is suppressed). Although much better agreement can be obtained when the parameter values are fixed by comparing the experimental data for just one steel with theory, this procedure is not justified because the parameters appear to vary haphazardly with alloy chemistry.

Acknowledgments

The authors are grateful to Professor C. J. Humphreys for the provision of laboratory facilities at the University of Cambridge. G. I. Rees gratefully acknowledges the support of the Science and Engineering Research Council and ESAB AB (Sweden). H. K. D. H. Bhadeshia's contribution to this work was made under the auspices of the 'Atomic Arrangements: Design and Control' project, which is a collaborative effort between the University of Cambridge and the Research and Development Corporation of Japan.

References

1. H. K. D. H. BHADESHIA: in 'Steel technology international', 289–294; 1989, London, Sterling Publications.
2. D. V. EDMONDS and R. C. COCHRANE: *Metall. Trans.*, 1990, **21A**, 1527–1540.
3. T. KO and S. A. COTTRELL: *J. Iron Steel Inst.*, 1952, **172**, 307–313.

4. H. K. D. H. BHADESHIA and D. V. EDMONDS: *Metall. Trans.*, 1979, **10A**, 895–907.
5. H. K. D. H. BHADESHIA and D. V. EDMONDS: *Acta Metall.*, 1980, **28**, 1265–1273.
6. R. F. HEHEMANN: in 'Phase transformations', 397–432; 1970, Metals Park, OH, ASM.
7. J. W. CHRISTIAN and D. V. EDMONDS: in 'Phase transformations in ferrous alloys', (ed. A. R. Marder and J. I. Goldstein), 293–327; 1984, Warrendale, PA, TMS-AIME.
8. H. K. D. H. BHADESHIA and J. W. CHRISTIAN: *Metall. Trans.*, 1990, **21A**, 767–797.
9. H. K. D. H. BHADESHIA: in 'Phase transformations in ferrous alloys', (ed. A. R. Marder and J. I. Goldstein), 335–340; 1984, Warrendale, PA, TMS-AIME.
10. A. ALI and H. K. D. H. BHADESHIA: *Mater. Sci. Technol.*, 1989, **5**, 398–402.
11. R. H. GOODENOW, S. J. MATAS, and R. F. HEHEMANN: *Trans. AIME*, 1963, **227**, 651–658.
12. G. R. SPEICH and M. COHEN: *Trans. AIME*, 1960, **218**, 1050–1059.
13. M. M. RAO and P. G. WINCHELL: *Trans. AIME*, 1967, **239**, 956–960.
14. H. K. D. H. BHADESHIA: *J. Phys. (Orsay)*, 1982, **43**, (C4), 443–448.
15. H. K. D. H. BHADESHIA: *Acta Metall.*, 1981, **29**, 1117–1130.
16. C. L. MAGEE: in 'Phase transformations', 115–156; 1970, Metals Park, OH, ASM.
17. G. B. OLSON and M. COHEN: *Metall. Trans.*, 1976, **7A**, 1897–1923.
18. H. K. D. H. BHADESHIA: *Met. Sci.*, 1982, **16**, 159–165.
19. A. ALI and H. K. D. H. BHADESHIA: *Mater. Sci. Technol.*, 1990, **6**, 781–784.
20. J. W. CHRISTIAN: 'Theory of transformations in metal and alloys', part I, 2 edn; 1975, Oxford, Pergamon.
21. R. T. DEHOFF and F. N. RHINES (eds): 'Quantitative microscopy', 1968, New York, NY, McGraw–Hill.
22. F. B. PICKERING: in Proc. Int. Conf. on 'Electron microscopy', 628–637; 1958, Berlin, FRG, Springer Verlag OHG.
23. Y. OHMORI, H. OHTANI, and T. KUNITAKE: *Trans. Iron Steel Inst. Jpn*, 1971, **11**, 250–259.

FUTURE DEVELOPMENTS OF

METALS AND CERAMICS

A collection of invited papers to mark the 70th birthday of Professor Sir Robert Honeycombe

Edited by J A Charles, G W Greenwood and G C Smith

This volume contains the invited papers presented at a meeting at the Royal Society in 1991 to honour Sir Robert Honeycombe's seventieth birthday and to mark his many contributions to materials science. Twelve papers cover the broad themes of materials' properties, processing and microstructure and assess the ways in which these areas are continuing to develop and are likely to move in the future.

Contents

- Preface
- Welcoming Comments
- Advanced Light Alloys
- High-Strength Steels
- Microalloyed Steels
- The Importance of Microstructural Characterisation in Improving Ceramics Engineering Applications
- Thermomechanical Processing
- Casting Technology
- Powders and Direct Metal Processing
- Welding Stainless Steels
- Laser Surface Treatments
- Electron Materialography
- Metals and Ceramics - Mechanical Properties
- Microstructural Refinement of Duplex Stainless Steels
- Concluding Remarks
- Professor Sir Robert Honeycombe: Published Works

Book 518 234x156mm 376pp (H) 0 901716 03 0 1992 £55.00 US$110.00 (Students: £25.00 US$50.00)

Orders with remittance* to: The Institute of Materials, Sales & Marketing Dept., 1 Carlton House Terrace, London SW1Y 5DB. Tel. 071-976 1338 Fax. 071-839 2078

Orders originating in Canada and the United States should be sent direct to: Ashgate Publishing Co., Old Post Road, Brookfield, VT 05036, USA. Tel (802) 276 3162 Fax. (802 276 3837

***Carriage: UK customers please add £2.50 per order, overseas customers add US$6.00**